R1/2

The influence of rounded edges on indentation by a flat punch

M Ciavarella[1], D A Hills[2] and G Monno[1]
[1]Dipartimento di Progettazione e Produzione Industriale, Politecnico di Bari, Italy
[2]Department of Engineering Science, University of Oxford

Abstract: The contact problem and stress state for indentation by a flat punch with rounded edges is studied. For the contact problem itself analytical solutions are obtained for both surface pressure and interior stress fields. Cases of normal indentation and frictional contact, the latter in both sliding or partial slip conditions, are all treated.

The transition from the Hertzian configuration to the contact between a nominally flat pad and contacting flat surface is discussed, and it is found that the strength of the contact decays surprisingly slowly. Regarding the von Mises yield parameter, there is a range of configurations for which the strength is actually higher than the Hertzian one, and the strength decays only when the corner radii are very small. The present solution is therefore a realistic alternative to the classical rigid-flat punch idealization, and has particular application to fretting fatigue tests.

Keywords: contact stresses, flat punch, fretting fatigue pads

1 INTRODUCTION

Indenters having a nominally flat end are frequently found both in experiments and in engineering practice. They often bear on a counterface that is also flat. Examples are readily found in fretting fatigue experiments, in indentation testing of glasses and ceramics, in support feet for all manner of equipment and in electrical brushes. In each of these problems contacts arise that characteristically have a flat base, with some kind of radius at the edge, which is either pre-existing or generated by wear. Further examples occur in the foundations of buildings or pads used to distribute load, e.g. under jacks. The design procedure for these contacts is usually one derived from experience, as it is notoriously difficult to determine the contact pressure, in contrast to, for example, the Hertzian contact, where simple closed-form solutions exist. Further, the use of flat-ended indenters, in both the fretting fatigue tests and fracture toughness indentation tests cited, demand a very precise knowledge of the internal stress state induced, as well as the contact pressure distribution.

Often the sides of the 'indenter' are straight and normal to the free end, and a deduction of the contact stress state induced is not a straightforward matter. The solution most often encountered is that due to Boussinesq [see, for example, Timoshenko and Goodier (1)], in which it is assumed that the indenter itself is rigid and is pressed into a compliant half-plane. The contact deformation is therefore accommodated entirely within the latter, and a classical formulation may be employed. As the contact is complete, the pressure distribution at the edges of the contact must be square root singular ($\sigma_{ij} \sim 1/\sqrt{r}$), and hence so are components of the stress field itself. This is physically unrealistic, even if the indenter is much stiffer than the substrate, and the singular state of stress would be relieved by limited-scale plasticity in either component. If the indenter and substrate have comparable elastic constants, the use of a half-plane formulation is, in any case, inappropriate, as there is no material adjacent to the contact to provide support; an elasticity formulation appropriate to a rectangular domain must therefore be used (2). Difficulties encountered in the Khadem and O'Connor analysis (2) are that the solution is in the form of a slowly convergent series and the geometry of the indenter remote from the contact itself has a significant effect on the contact pressure distribution, which is not observed experimentally.

For perfectly flat contacts, the interfacial contact pressure is hypersensitive to small variations in surface geometry, particularly the presence of swarf near the edge of the indenter. If, however, the corners of the punch are rounded off, as shown in Fig. 1, most of these problems disappear; there is much less tendency for swarf to become trapped, the contact pressure falls

The MS was received on 18 March 1997 and was accepted for publication on 13 October 1997.

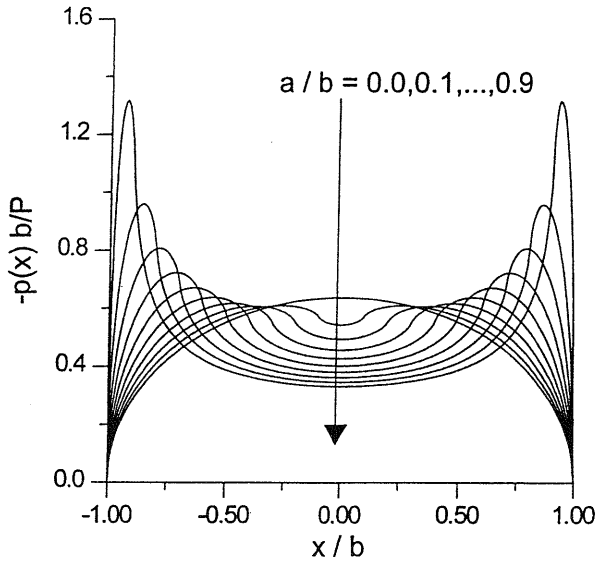

Fig. 2 Pressure distributions: $a/b = 0.0, 0.1, \ldots, 0.9$

the value $1/\pi$, predicted by the rigid punch singular solution, showing that the difference in behaviour as the limit $a/b \to 1$ is approached is concentrated at the edges of the contact.

3.2 Partial slip contact: loading

So far the case of normal loading has been considered, i.e. a central normal force was applied to the indenter and, for elastically similar contacts, the pressure distribution under such conditions has been found. Attention is now turned to the sequential loading of a tangential force. In particular, after the normal load P is applied, P is kept constant and a monotonically increasing tangential force Q, less than that needed to cause sliding, is applied. This analysis applied only to the case where the contact arises between elastically similar components. In order to determine the stick/slip zone geometry a second integral equation needs to be considered, which relates the displacement of particles parallel with the surface to the surface tractions [see reference (7), p. 53, equation 2.22], viz.

$$\frac{E^*}{2} g'(x) = \frac{1}{\pi} \int_L \frac{q(\xi)\,\mathrm{d}\xi}{x-\xi} + \beta p(\xi) \tag{12}$$

where $g(x)$ is the relative tangential displacement of surface particles and $g'(x) = \mathrm{d}g(x)/\mathrm{d}x$ its derivative. Tangential equilibrium will be satisfied if

$$Q = \int_L q(\xi)\,\mathrm{d}\xi \tag{13}$$

As stated at the outset, Dundurs' constant is assumed to vanish, so that both equations (1) and (12) take on simplified appearances and become uncoupled. The following equations may be used to establish the size of the stick zone, c, which must be centrally positioned, from considerations of symmetry.

Within the stick zone the relative tangential displacement of surface particles must be zero, since there was no relative displacement cumulated during the phase of normal loading, so that

$$g'(x) = 0, \qquad -c < x < c \tag{14}$$

and the shearing traction must be less than the limiting value, i.e.

$$|q(x)| < -fp(x), \qquad -c < x < c \tag{15}$$

where f is the coefficient of friction. Further, within the slip zones the shearing traction is limited by friction, so that

$$q(x) = fp(x), \qquad \begin{cases} -b < x < -c \\ +c < x < +b \end{cases} \tag{16}$$

Basic energetic considerations also state that the shear traction must always locally oppose the direction of change of the slip displacement, i.e.

$$\operatorname{sgn}[q(x)] = \operatorname{sgn}\left(\frac{\partial q}{\partial t}\right), \qquad \begin{cases} -b < x < -c \\ +c < x < +b \end{cases} \tag{17}$$

Upon applying a normal load, P, alone, there is no tendency for surface particles to slip, and hence the initial stick zone envelops the entire contact. A monotonically increasing shearing force, Q, will therefore give rise to advancing slip, and under these circumstances equation (17) is automatically satisfied. The shear tractions arising in the contact will be considered as a superposition of the full sliding one, with a 'difference' part, $q^*(x)$. Two cases need to be considered separately, viz. when the dimension of the stick zone, c, is less than the dimension of the flat part of the indenter, b, and the case $c > b$.

In the first case $c < b$, equation (12) states that

$$\frac{E^*}{2} g'(x) = 0 = \frac{1}{\pi} \int_L \frac{fp(\xi) + q^*(\xi)\,\mathrm{d}\xi}{x-\xi} = \frac{1}{\pi} \int_{L_{\text{stick}}} \frac{q^*(\xi)\,\mathrm{d}\xi}{x-\xi}, \qquad -b < -c \leqslant x \leqslant c < b \tag{18}$$

The second, simplified, term in the above equation follows from equation (1), which indicates that the first term in the first integral is proportional to $h'(x)$, and is zero for $|x| < a$. Then, because only bounded solutions can be considered [as $q^*(x)$, being a perturbation within the stick zone, must fall continuously to zero at the stick/slip boundary], only the solution $q^*(x) = 0$ is compatible with the present model. This simply means that, within the limit of the half-plane assumptions, no partial slip solution can exist when the stick zone is contained

entirely within the flat part of the punch. It should be borne in mind that this conclusion has been arrived at within the context of a half-plane formulation, and in a real problem the presence of far boundaries *may* have an influence on the solution. Nevertheless, the solution presented is a strong indication that there is unlikely to be a stable partial slip solution in this regime.

Attention is now turned to the case where the stick zone at the maximum shearing force extends into the curved portion of the indenter profile ($c > b$). Again the shearing stress is represented as the sum of the full slip solution together with a perturbation in the stick zone, and if the corresponding integral is split into two parts, the term relating to the full slip distribution is seen to be the same as equation (1). This immediately allows the following simplified integral equation for $q^*(x)$ to be written:

$$\frac{1}{\pi}\int_{L_{\text{stick}}} \frac{q^*(\xi)\,\mathrm{d}\xi}{x-\xi} = -\frac{E^* f}{2}\begin{cases} -(a+x)/R, & -c \leqslant x \leqslant -a \\ 0, & -a \leqslant x \leqslant +a \\ -(x-a)/R, & +a \leqslant x \leqslant +c \end{cases} \quad (19)$$

Thus, the same integral equation arising for normal loading must be solved to determine the influence of the corrective tangential shearing traction, $q^*(x)$. The results presented in Section 3.1 therefore apply, *mutatis mutandis*. If the actual shearing force is Q, the value of the corrective shearing force, Q^*, corresponding to the corrective tractions is given by $Q^* = Q + fP$, and the auxiliary angle θ is used to define x. The necessary changes are that Q'/f replaces P, θ replaces ϕ, θ_0 replaces ϕ_0 and c replaces b. It should be stated that when the length of the flat portion of the contact is made vanishingly small, $a \to 0$, the standard Cattaneo–Mindlin solution (**9**, **10**) is recovered. It will be recognized that this argument may be used for an indenter of *any* shape.

It is interesting to look at the relationship between applied dimensionless shearing force, $Q/(fP)$, and the non-dimensional stick zone size, c/b. From the considerations above, it can easily be shown that, for the geometry under consideration,

$$\frac{|Q|}{fP} = 1 - \left(\frac{c}{b}\right)^2 \frac{\pi - 2\theta_0 - \sin 2\theta_0}{\pi - 2\phi_0 - \sin 2\phi_0}, \qquad c > a \quad (20)$$

whereas $Q/(fP) = 1$ for $c \leqslant a$. This relationship is shown in Fig. 3, where it may be appreciated that, in the partial slip regime, c cannot be smaller than a. This simply means that the transition partial slip–sliding is reached when the slip zone envelopes the rounded part of the contact, but it may be observed that this transition is smooth, both in the value of $Q/(fP)$ and its derivative. The solution for $a/b = 0$, the Hertzian geometry, and hence the Cattaneo–Mindlin problem, is included for comparison. Note also that as a/b is increased, so that the geometry tends to the flat-ended rigid punch case, the stick-slip behaviour of the completely flat contact is recovered, so that there is no stable partial slip regime.

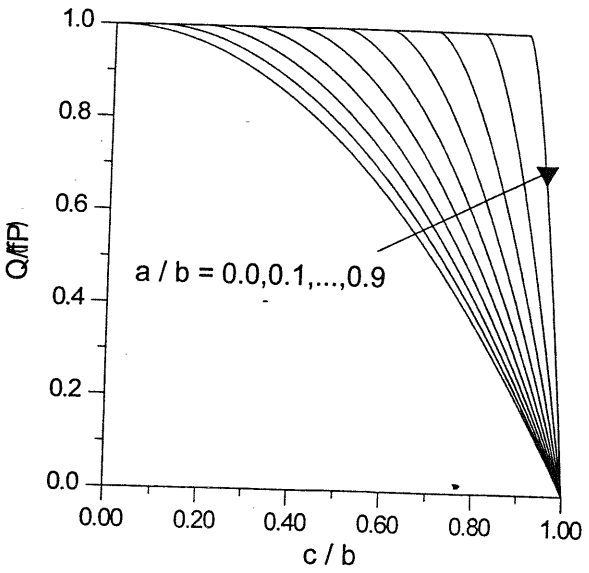

Fig. 3 Partial slip problem: relationship between applied shearing force $Q/(fP)$ and stick zone size c/b

3.3 Partial slip contact: unloading and cyclic loading

The procedure outlined above may be extended to the unloading configuration. Suppose that a particular partial slip condition has been reached in loading, corresponding to a tangential load $Q_{\max}$, with a stick zone L_{stick} of dimension $2c_{\max}$. At the start of unloading, stick occurs everywhere. On further reducing the value of the tangential load, reverse slip occurs at the edge of the contact area. The configuration is again one of advancing slip, according to Dundurs' classification, and therefore the problem does not require an incremental formulation.

Define a particular unloading level, Q ($< Q_{\max}$), with a new stick zone $L^{\text{u}}_{\text{stick}}$ of dimension $2d$. The new traction distribution can be found from a superposition of the previous one at the end of loading phase, plus a full reverse slip distribution and a new corrective part $q^{**}(x)$. The considerations rehearsed for the loading case continue to apply, and using equation (12) (with $\beta = 0$), the amount of slip that is 'locked in' the slip zones at the end of the normal loading phase can be calculated. It may easily be shown that this new corrective component is again of the same form as the normal contact pressure, rescaled for the dimension of the new stick zone. Therefore, the correction is zero if the new stick zone is entirely within the flat part of the contact, which again means that during unloading, as for loading, a partial slip regime is not possible with the stick zone lying entirely within the flat part of the contact.

It is clear that the same procedure can be continued

for cyclic loading, whereas more complicated laws of loading, such as oblique loading or reloading from an incompletely reversed unloading, require special investigation and are not within the scope of the present paper.

4 INTERIOR STRESS FIELD

The strength of the contact, as quantified by a resistance to yielding, demands a knowledge of the complete interior stress field, as, particularly for low coefficients of friction, the strength is controlled by a subsurface point. The most suitable vehicle to use for half-plane problems is Mushkelishvili's potential, and it is very straightforward to include the effects of sliding friction, as the shearing traction distribution is identical to the contact pressure. Furthermore, as it has been shown, the 'corrective' term in the case of partial slip problems also has the same form, and hence it is equally straightforward to determine the stress state in the case of partial slip problems.

As the shear traction in the full sliding regime is $q(x) = fp(x)$ throughout the whole contact, Mushkelishvili's potential is given by

$$\Phi(z) = \frac{1 - if}{2\pi i} \int_{-1}^{1} \frac{p(t)}{t - z} \, dt \tag{21}$$

where dimensionless coordinates are now adopted for $x, y, t, z = x + iy$ by normalizing them with respect to the contact half-width b, and $p(x)$ is expanded in terms of Chebyshev polynomials $U_{2n}(x)$ as

$$p(x) = -\sqrt{(1 - x^2)} \sum_{n=0}^{\infty} b_n U_{2n}(x) \tag{22}$$

The corresponding Mushkelishvili's potential is (7)

$$\Phi(z) = \frac{1 - if}{2\pi i} \int_{-1}^{1} \frac{p(t)}{t - z} \, dt = -\frac{i + f}{2} \sum_{n=0}^{\infty} b_n R_{2n+1}(z) \tag{23}$$

where $R_n(z) = [z - (z^2 - 1)^{1/2}]^n$. From the potential, the stresses can be obtained using the standard relations

$$\frac{\sigma_x + \sigma_y}{2} = 2Re\, \Phi(z)$$

$$\frac{\sigma_y - \sigma_x + 2i\tau}{2} = (\bar{z} - z)\Phi'(z) - \bar{\Phi}(z) - \Phi(z)$$

as well as the displacement derivatives. The absolute displacements may be found only to within an arbitrary constant, which is a characteristic of plane elasticity.

5 RESULTS

5.1 Yield strength

It is difficult to display comprehensive results for the complete state of stress over the neighbourhood of contact with several independent variables. These are the ratio of the size of the straight part of the punch to the end radius, a/R, or, equivalently, the dimensionless size of the contact, b/a, the coefficient of friction, f, and, if the contact is in partial slip, the dimensionless shearing force, $Q/(fP)$. Results have therefore been chosen to illustrate the frictionless case and $f = 0.3$, which is representative of the measured value in many instances. Moreover, the investigation will be limited to the value of Poisson's ratio equal to 0.3, which is the value of greatest engineering interest.

Figure 4 shows plots of the normalized von Mises yield parameter, $b\sqrt{J_2}/P$, for representative cases. As the ratio a/R becomes very small the solution tends to the standard Hertzian distribution, while as R/a becomes small the geometry looks increasingly like a flat-ended punch. However, perhaps surprisingly, the strength of the contact first *increases* with respect to the Hertzian case and then decreases very slowly. Results from several plots of this kind are summarized in Fig. 5, which gives the elastic limit for normal indentation as a function of the ratio b/a according to von Mises' yield criterion, with the yield strength of the material in pure shear being denoted by k. Also shown in the figure is the depth at which the severest state of stress occurs, and therefore the point at which the yield condition is first attained. It will be recognized that over the wide range $0 < a/b < 0.55$ the contact strength is in fact higher than the Hertzian case (or the state of stress is milder) for normal frictionless contact. The reason for this is apparent from a consideration of Fig. 2, where the pressure is close to uniform over a wide range of geometries and the maximum of the yield parameter $b\sqrt{J_2}/P$ moves from a point at the centre-line to a *region* of near-maximum value, located well off-axis. If the ratio a/b is increased further, the strength of the contact drops rapidly, and is almost halved for a ratio of $a/b \approx 0.9$. In some respects much more useful design information can be obtained from these calculations than the Boussinesq solution, which suggests that (admittedly for an atomically sharp contact) the elastic limit is zero.

For design purposes, a complete set of results has been obtained for the full sliding case, which are summarized in Fig. 6 for a more complete range of values of $a/b = 0, 0.9$, in steps of 0.05. The dashed line represents the well-known Hertzian case (7), whereas the lines $a/b = 0.05, 0.1, 0.15, 0.2$ are a little higher than the Hertzian line for low values of f, when the strength is subsurface controlled, and fall well below the Hertzian line for $f \geqslant 0.3$. This behaviour is better understood from Fig. 7, where the locus of the severest state of stress is shown. First, starting from the Hertzian configuration, for coefficients of friction less than about $f = 0.3$ the severest state of stress remains subsurface, while for higher values of f the tendency to yield is greatest at the surface, in the sense that the local maximum on the surface suddenly becomes the global maximum. This behaviour

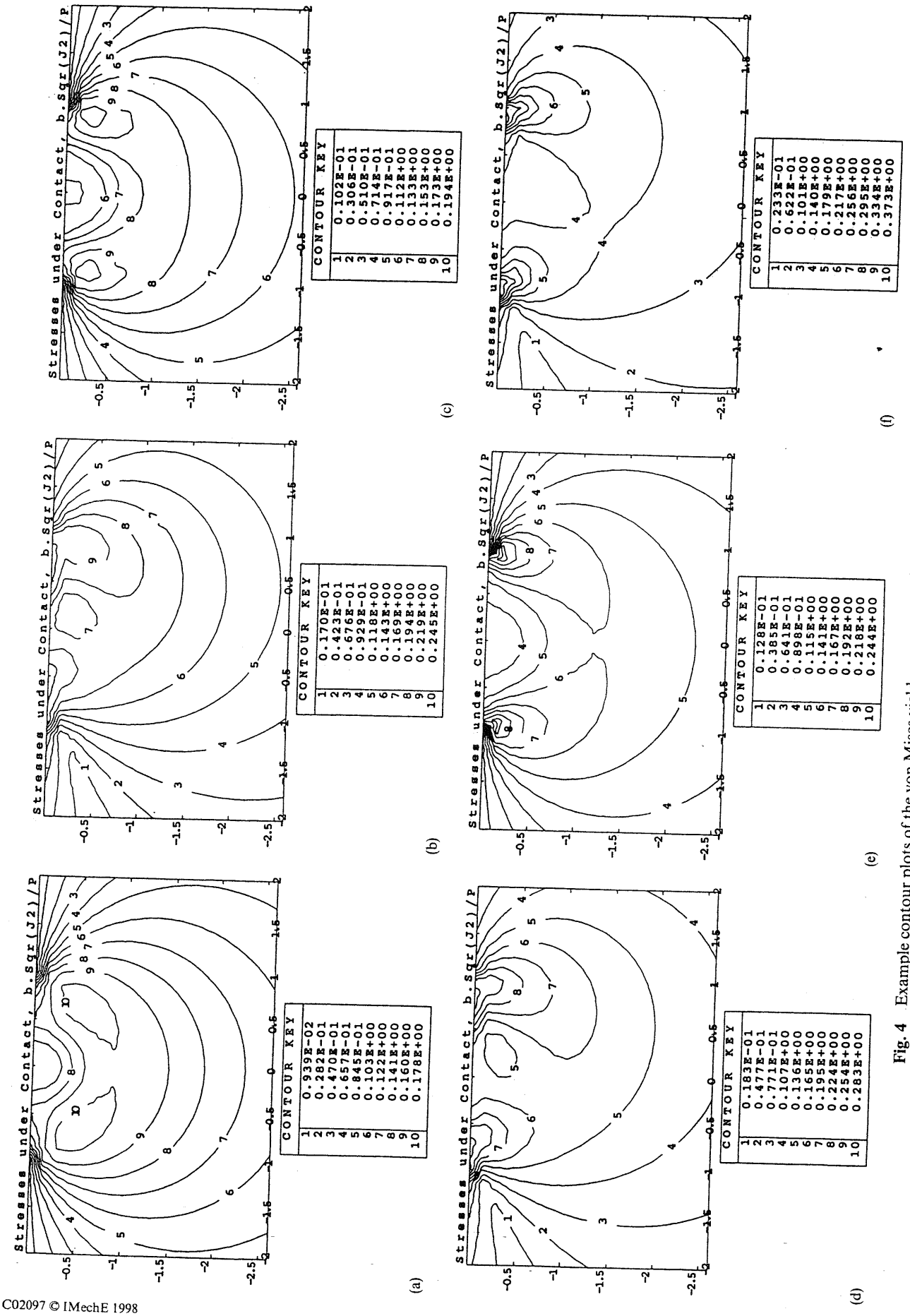

Fig. 4 Example contour plots of the von Mises yield parameter under sliding conditions $b\sqrt{J_2}/P$ for (a) $a/b = 0.3$, $f = 0.0$, (b) $a/b = 0.3$, $f = 0.3$, (c) $a/b = 0.55$, $f = 0.0$, (d) $a/b = 0.55$, $f = 0.3$, (e) $a/b = 0.8$, $f = 0.0$, (f) $a/b = 0.8$, $f = 0.3$ ($\nu = 0.3$)

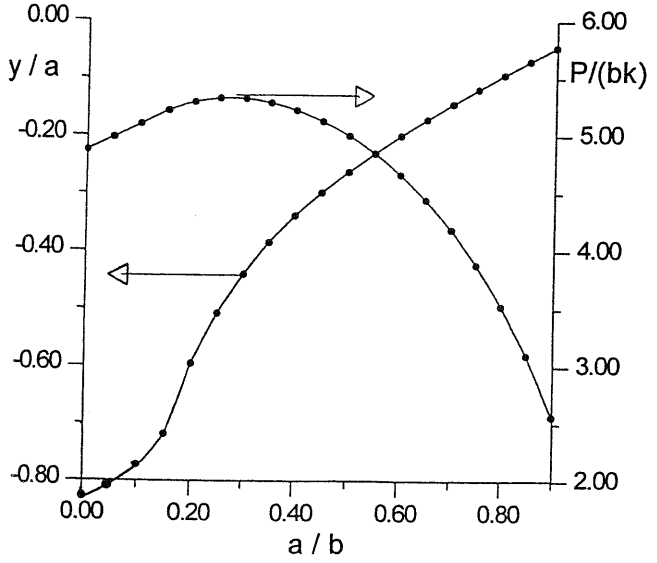

Fig. 5 Elastic limit $P/(bk)$ for normal indentation, including the depth of the severest state of stress, as a function of a/b ($\nu = 0.3$)

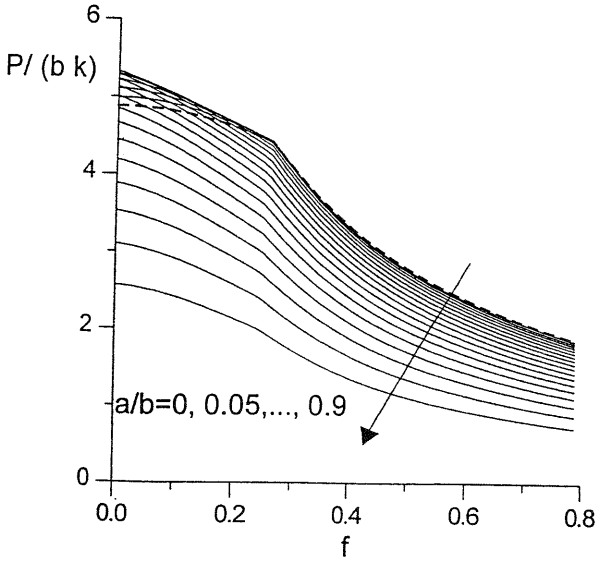

Fig. 6 Elastic limit $P/(bk)$ for sliding indentation as a function of a/b and the coefficient of friction f ($\nu = 0.3$)

gives rise to the cusp shape of the dashed line in Fig. 6 and corresponds, in Fig. 7, to the jump of the point where the overall maximum moves to the surface (in Fig. 7 each small cross corresponds to an increase of $f = 0.0125$). For the rounded flat punch case, for low a/b ratios the point at which yield first occurs is deeper, but persists at a subsurface point for longer, before jumping to the surface. For $a/b < 0.2$, the lateral (x value) of the point of severest stress increases significantly for low coefficients of friction and, for $f > 0.3$, the point moves to the surface. For higher a/b ratios, the strength gradually decreases and, when compared with the normal loading, the decrease in strength is proportionately greater.

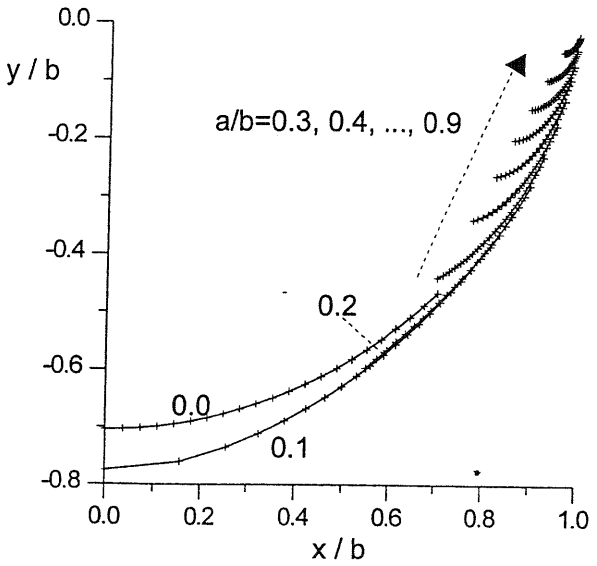

Fig. 7 Location of the maximum of the von Mises yield parameter $b\sqrt{J_2}/P$ in the subsurface case for sliding indentation as a function of a/b and the coefficient of friction f (each little cross corresponds to an increment of $f = 0.0125$) ($\nu = 0.3$)

5.2 Fatigue and brittle fracture strength of the contact

One of the principal practical applications of the analysis is the use of almost flat-ended pads on fretting fatigue specimens, where the ratio a/R might typically be about 10. The geometry is operated in the partial slip regime, with the shearing force being generated by imposing a small tangential displacement, either using a rotating–bending or push–pull arrangement (11). In these cases, although the yield condition is important, the most important quantity, and the one that controls the development and growth of cracks, is the maximum tensile stress; of particular relevance is its value at or near the surface, adjacent to the trailing edge of the contact, where its maximum value occurs. Figure 8 summarizes the results for maximum surface tension, for a partial slip or full sliding contact, as a function of c/b [equivalently, in terms of $q/(fP)$, see Fig. 3] and for a range of geometries, a/b. The maximum tension is lower for a partial slip configuration, which is clear from the fact that the resulting applied tangential load is lower. In the Hertzian case, the decrease in surface tension is immediate and occurs as soon as c/b (dimensionless size of the stick zone) increases from zero; in the flat punch case, the decrease starts to occur when $c/b \geqslant a/b$, simply because the contact is in full sliding for lower c/b.

If the stress concentration for surface tension is considered as a function of Q, it is clear that the full sliding condition is less severe than the full-stick case, which arises only when the coefficient of friction is infinitely high. The flat punch case is always more severe than the Hertzian case, although for a/b as high as 0.8, the stress concentration is only double the Hertzian case.

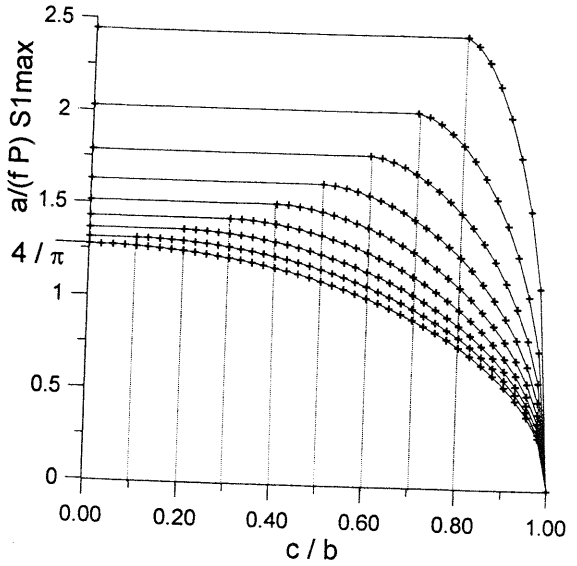

Fig. 8 Maximum tension arising in the surface under partial slip conditions

6 CONCLUSIONS

The problem of a flat punch with rounded edges has been studied in detail, giving analytical results for surface traction and interior stress field induced by the contact. This changes the character of the solution compared with a punch having abrupt corners, for which the strength of the contact is not clearly defined. It has the advantages, from both the analytical and experimental viewpoints, of producing a well-defined state of stress and a quantifiable partial slip solution. It is also worth remarking that the geometry is the only one of simple manufacture that renders the contact, under a wide range of loading conditions, less severe than the Hertzian one. If the contact also transmits tangential loading, the concentration of tensile stresses at the trailing edge of a sliding contact is shown to be always significantly higher than the Hertzian case, but the transition to the infinitely high stress concentration associated with a sharp-cornered flat punch is slow. For design purposes, a complete set of practical diagrams has been given.

REFERENCES

1 **Timoshenko, S. P.** and **Goodier, J. N.** *Theory of Elasticity*, 2nd edition, 1951 (McGraw-Hill, New York).

2 **Khadem, R.** and **O'Connor, J. J.** Adhesive or frictionless compression of an elastic rectangle between two identical elastic half-spaces. *Int. J. Engng Sci.*, 1969, 7, 153–168.

3 **Goodier, J. N.** and **Loutzenheiser, C. B.** Pressure peaks at the ends of plane strain rigid die contacts (elastic). *J. Appl. Mech.*, 1965, **32**, 462–463.

4 **Galin, L. A.** *Contact Problems in the Theory of Elasticity*, 1953 (Gostekhizdat, Moscow). English translation by Department of Mathematics, North Carolina State College, Raleigh.

5 **Steuerman, I. Ya.** *Contact Problem of the Theory of Elasticity*, 1949 (Gostekhteoretizdat, Moscow and Leningrad). Available from the British Library in an English translation by Foreign Technology Division, FTD-MT-24-61-70, 1970.

6 **Mushkelishvili, N. I.** *Singular Integral Equation* (Translated by J. R. M. Radok), 1977 (Noordhoff International Publishing).

7 **Hills, D. A., Nowell, D.** and **Sackfield, A.** *Mechanics of Elastic Contacts*, 1993 (Butterworth-Heinemann, Oxford).

8 **Sackfield, A.** and **Hills, D. A.** Sliding contact between dissimilar elastic bodies. *J. Tribology*, 1988, **110**(4), 592–596.

9 **Cattaneo, C.** Sul contatto di due corpi elastici: distribuzion locale degli sforzi. *Reconditi dell Accademia nazionale dei Lincei*, 1938, **27**, 342–348, 434–436, 474–478.

10 **Mindlin, R. D.** Compliance of elastic bodies in contact. *J. Appl. Mech.*, 1949, **16**, 259–268.

11 **Hills, D. A.** and **Nowell, D.** The development of a fretting fatigue experiment with well-defined characteristics. In *Standardization of Fretting Fatigue Test Methods and Equipments*, ASTM STP 1159 (Eds M. Helmi Attia and R. B. Waterhouse), 1992, pp. 33–48 (American Society for Testing and Materials, Philadelphia, Pennsylvania).

APPENDIX

Derivation of the pressure distribution

From the integral relating the pressure to the function $h'(t)$, equation (5) in the main text,

$$p(x) = -\frac{E^*}{2\pi R}\sqrt{(b^2-x^2)}\left[\int_{-b}^{-a}\frac{(a+t)\,\mathrm{d}t}{\sqrt{(b^2-t^2)}(t-x)} + \int_{a}^{b}\frac{(t-a)\,\mathrm{d}t}{\sqrt{(b^2-t^2)}(t-x)}\right] \quad (24)$$

On adding and subtracting x, this becomes

$$p(x) = -\frac{E^*}{2\pi R}\sqrt{(b^2-x^2)} \times \left[(a+x)\int_{-b}^{-a}\frac{\mathrm{d}t}{\sqrt{(b^2-t^2)}(t-x)} + \int_{-b}^{-a}\frac{\mathrm{d}t}{\sqrt{(b^2-t^2)}} + \int_{a}^{b}\frac{\mathrm{d}t}{\sqrt{(b^2-t^2)}} + (x-a)\int_{a}^{b}\frac{\mathrm{d}t}{\sqrt{(b^2-t^2)}(t-x)}\right] \quad (25)$$

Now,

$$\int_{-b}^{-a}\frac{\mathrm{d}t}{\sqrt{(b^2-t^2)}} = \int_{b}^{a}\frac{\mathrm{d}t}{\sqrt{(b^2-t^2)}} = \frac{\pi}{2} - \phi_0$$

where $\phi_0 = \arcsin a/b$. Further, define $t = [2\tau/(1+\tau^2)]b$ and $x = [2\xi/(1+\xi^2)]b$, so that

$$\int_{x_1}^{x_2} \frac{\mathrm{d}t}{\sqrt{(b^2-t^2)(t-x)}}$$

$$= \frac{1+\xi^2}{b} \int_{\xi_1}^{\xi_2} \frac{\mathrm{d}\tau}{(\tau-\xi)(1-\tau\xi)} \tag{26}$$

$$= \frac{1+\xi^2}{b(1-\xi^2)} \left(\int_{\xi_1}^{\xi_2} \frac{\mathrm{d}\tau}{\tau-\xi} - \int_{\xi_1}^{\xi_2} \frac{\mathrm{d}\tau}{\tau-1/\xi} \right) \tag{27}$$

where ξ_1, ξ_2 are related to x_1, x_2 by

$$x_1 = \frac{2\xi_1}{1+\xi_1^2} b, \qquad x_2 = \frac{2\xi_2}{1+\xi_2^2} b \tag{28}$$

Now, considering the Cauchy principal values of the integrals of the last formula,

$$-\int_{x_1}^{x_2} \frac{\mathrm{d}t}{\sqrt{(b^2-t^2)(t-x)}}$$

$$= \frac{1+\xi^2}{b(1-\xi^2)} \ln \left| \left(\frac{\xi-\xi_2}{\xi-\xi_1} \right) \left(\frac{1-\xi\xi_1}{1-\xi\xi_2} \right) \right| \tag{29}$$

Assuming $\xi = \tan \phi/2$ and substituting, with integration limits given by

$$x_1 = -b, \quad x_2 = -a, \quad \xi_1 = -1, \qquad \xi_2 = -\tan \frac{\phi_0}{2}$$

$$x_1 = a, \qquad x_2 = b, \qquad \xi_1 = \tan \frac{\phi_0}{2}, \quad \xi_2 = 1 \tag{30}$$

it is found that

$$\int_{-b}^{-a} \frac{\mathrm{d}t}{\sqrt{(b^2-t^2)(t-x)}} = \frac{1}{b\cos\phi} \ln \left| \frac{\sin(\phi+\phi_0)/2}{\cos(\phi-\phi_0)/2} \right|$$

$$\int_{a}^{b} \frac{\mathrm{d}t}{\sqrt{(b^2-t^2)(t-x)}} = \frac{1}{b\cos\phi} \ln \left| \frac{\cos(\phi+\phi_0)/2}{\sin(\phi-\phi_0)/2} \right| \tag{31}$$

From equations (28) and (30), it follows that $x = b \sin \phi$, and assuming $a = b \sin \phi_0$ and substituting gives

$$\frac{2\pi R}{aE^*} p(\phi) = -(\pi - 2\phi_0) \frac{\cos\phi}{\sin\phi_0} - \frac{\sin\phi}{\sin\phi_0} \ln \left| \frac{\sin(\phi+\phi_0)}{\sin(\phi-\phi_0)} \right| - \ln \left| \tan \frac{\phi+\phi_0}{2} \tan \frac{\phi-\phi_0}{2} \right| \tag{32}$$

Overall equilibrium is ensured by substituting the profile dervative into equation (6):

$$\frac{2PR}{E^*} = \int_{-b}^{-a} \frac{(a+t)t\,\mathrm{d}t}{\sqrt{(b^2-t^2)}} + \int_{a}^{b} \frac{(t-a)t\,\mathrm{d}t}{\sqrt{(b^2-t^2)}} \tag{33}$$

Assuming $t = b \sin \phi$ and according to $a = b \sin \phi_0$, the integration is straightforward and gives

$$\frac{2PR}{E^*} = \int_{-\pi/2}^{-\phi_0} (\sin\phi_0 + \sin\phi) \sin\phi \, \mathrm{d}\phi + \int_{\phi_0}^{\pi/2} (\sin\phi - \sin\phi_0) \sin\phi \, \mathrm{d}\phi \tag{34}$$

$$= a^2 \left(\frac{\pi - 2\phi_0}{2\sin^2\phi_0} - \cot\phi_0 \right) \tag{35}$$